Adsorption 4, 159–172 (1998)

Periodic State Heat Effects in Pressure Swing Adsorption-Solvent Vapor Recovery

YUJUN LIU AND JAMES A. RITTER
Department of Chemical Engineering, Swearingen Engineering Center, University of South Carolina, Columbia, South Carolina 29208
Ritter@sun.che.sc.edu

Abstract. Heat effects in the pressure swing adsorption (PSA)-*n*-butane vapor recovery process were investigated at the periodic state by computer simulation. The PSA process utilized a two-bed, four-step, vacuum swing cycle and BAX activated carbon as the adsorbent. The heat effects were manifested by varying the heat transfer coefficient (h) from isothermal to adiabatic, while simultaneously varying the adsorbed phase heat capacity (Cp_a) from zero to that of the saturated liquid. In terms of the bed capacity factor (BCF), isothermal operation always resulted in the best performance, whereas adiabatic operation was not the worst; independent of Cp_a, the worst performance occurred at an intermediate h. Cp_a also had a significant effect on the BCF, where a larger Cp_a (i.e., a larger heat sink) always decreased the BCF and thus improved the process performance. A factorial analysis showed that the effect of Cp_a on the BCF became even more pronounced as the cycle time increased. h and Cp_a had essentially no effect on the solvent vapor enrichment under the conditions investigated. Overall, this study demonstrated that the effects of h and Cp_a are uniquely coupled; thus knowing their magnitudes is paramount to obtaining accurate predictions from a PSA-solvent vapor recovery model.

Keywords: computer simulation, butane, activated carbon, environmental, adsorbed phase heat capacity

Introduction

PSA has been studied extensively over the past three or four decades, with critical reviews and monographs given by Ruthven (1984), Tonduer and Wankat (1985), Wankat (1986), Yang (1987), and Ruthven et al. (1994), among others. Temperature swings have been reported in essentially all pressure swing adsorption (PSA) processes, ranging from a few degrees Celsius in purification (Farooq et al., 1988) and air drying (Chihara and Suzuki, 1983) to several tens of degrees Celsius in bulk gas separation (Yang and Doong, 1985; Doong and Yang, 1986; Cen and Yang, 1986). The general conclusion drawn from these studies and others is that non-isothermal effects are detrimental to the performance of nearly all PSA processes no matter how slight the temperature swings. As a result, numerous simulation studies have accounted for temperature effects in PSA processes (Chihara and Suzuki, 1983; Yang and Doong, 1985; Doong and Yang, 1986; Cen and Yang, 1986; Farooq et al., 1988; Mahle et al., 1996; Liu and Ritter, 1996, 1997a, 1997b), but only those by Chihara and Suzuki (1983), and Liu and Ritter (1997b) have provided direct evidence of heat effects by comparing isothermal with non-isothermal or adiabatic operation. The recent works by Liu and Ritter (1996, 1997a, 1997b) have also shown that heat effects in PSA-solvent vapor recovery (SVR) processes can be quite pronounced, and more significant than in conventional PSA separation and purification processes mainly because of the adsorbate characteristics.

PSA-SVR is a slightly modified version of conventional PSA in that the feed is supplied to the column at or near atmospheric pressure, and partial pressure reduction is accomplished by vacuum along with purging. Furthermore, very strong interactions or high affinities exist between the adsorbate and the adsorbent, which give rise to rather

large heats of adsorption; and because the adsorbate is usually a condensable vapor, PSA-SVR processes also experience very high loadings at relatively low partial pressures, with pore condensation an eminent possibility. These unique adsorbate-adsorbent characteristics suggest that the thermodynamics of the adsorbed phase may play a more significant role in PSA-SVR processes than in conventional PSA processes.

The thermodynamics of the adsorbed phase can be accounted for in a PSA model by including a term for the adsorbed phase heat capacity (Cp_a) in the energy balance. However, in most of the published PSA models, Cp_a has not been included, with exceptions given by Kapoor and Yang (1988) and Liu and Ritter (1997b). Kapoor and Yang (1988) assumed Cp_a to be the same as that of the gas phase, whereas Liu and Ritter (1997b) assumed Cp_a to be the same as that of the saturated liquid. These studies alone do not reveal the effect of Cp_a on the simulation results, but collectively they do reveal a degree of uncertainty about the state of the adsorbed phase, i.e., whether the adsorbate exists as a gas, liquid, solid, or something all together different lying somewhere in between one of these states. The Cp_a has been studied by several researchers (Hill, 1949; Berezin and Kiselev, 1966; Sircar, 1985); but the present state of knowledge is far from satisfactory from an engineering point of view.

Moreover, a comparison of the recent works by Liu and Ritter (1996, 1997a, 1997b) reveals qualitatively that the magnitude of the heat effect, at least in PSA-SVR processes, may change dramatically depending on whether Cp_a is included in the model or not. Because Cp_a acts as a heat sink and thus directly opposes the effects associated with the heat of adsorption, the heat effect was not as marked when Liu and Ritter included Cp_a in their model (1997b). However, the net heat effect depends ultimately on the non-isothermal nature of the PSA process, which in turn depends on the heat transfer characteristics of the process, which in turn depends on the size of the column. For example, as the diameter of the column increases, the operation changes from nearly isothermal to essentially adiabatic; and it is generally believed that adiabatic operation leads to the worst process performance (Chihara and Suzuki, 1983; Yang, 1987). But this may not be the case, especially if the heat of adsorption can be retained in the column to assist regeneration (Leavitt, 1962; White and Barkley, 1984).

Therefore, the objective of this study was to gain a fundamental understanding of how the heat effect is manifested in PSA processes, and also how the magnitude of the heat effect changes with certain process conditions. An extensive simulation study of a PSA-SVR process was carried out for this purpose, where the interplay between the overall heat transfer coefficient (h) and the Cp_a was examined. The *n*-butane vapor-nitrogen-BAX activated carbon system was studied because the heat effect in this system was anticipated to be significant (Liu et al., 1997); and butane vapor represents one of the light vapor components in gasoline vapor recovery operations (Tolles, 1996).

Process Description

A four-step, two-bed vapor recovery process was operated using commercially relevant PSA-SVR process conditions. Table 1 displays the process conditions, along with the bed characteristics and physical properties. The four steps consisted of (I)

Table 1. Bed characteristics, process conditions, and physical properties.

Bed radius (r_b)	0.0387 m
Bed length (L)	0.2724 m
Packing void fraction (ε)	0.391
Pellet density (ρ_p)	550.0 kg/m^3
Pellet radius (r_p)	0.00105 m
Heat capacity of adsorbent (Cp_s)	1.046 kJ/(kg K)
Heat of adsorption (ΔH)	−40.266 kJ/mol
Mass transfer coefficient (k)	0.0266 s^{-1}
Feed flow rate (V_f)	0.002 m^3/min
Feed mole fraction (y_f)	20%
Feed temperature (T_f)	300.4 K
Ambient temperature (T_0)	299.5 K
Feed pressure (P_H)	113.6 kPa
Purge pressure (P_L)*	15.1 kPa
Pressure ratio (α)	7.52
Purge to feed ratio (γ)	0.835
Total cycle time (t_c)	20 min
Cycle step time (t_s)	
I and III:	2 min
II and IV:	8 min

*Value of P_L taken at the end of step IV.

countercurrent pressurization with inert carrier gas (nitrogen), (II) cocurrent high pressure adsorption with feed, (III) countercurrent blowdown, and (IV) countercurrent low pressure desorption with light product purge. The carrier gas was purified during step II, whereas the solvent vapor was enriched and recovered in steps III and IV. The amount of purge gas used was determined by the purge to feed ratio, γ, which was defined as the ratio of the actual gas volume used for purge to the actual volume of the feed gas.

The PSA-SVR process performance at the periodic state was judged by four process performance indicators (Liu and Ritter, 1996): the solvent vapor recovery (R), solvent vapor enrichment (E), light product purity (y_p), and bed capacity factor (BCF). R was defined as the ratio of the number of moles of the solvent vapor leaving the bed during steps III and IV to the number of moles of the solvent vapor entering the bed during step II. E was defined as the average mole fraction of the solvent vapor leaving the bed during steps III and IV divided by the mole fraction of the feed solvent vapor. y_p was defined as the average mole fraction of the solvent vapor exiting the light product end of the bed during step II. BCF was defined as (Liu and Ritter, 1996)

$$\text{BCF} = \int_0^L q\, dz \,/\, q_f^* L \tag{1}$$

and represents the capacity of the bed that is used at the periodic state (measured at the end of step II) compared to the maximum capacity of the bed at the feed conditions. Thus, at a fixed process throughput and when there is no solvent vapor breaking through the bed during Step II, a larger BCF indicates a poorer performance.

To simulate environmental applications of PSA-SVR, the process conditions of this study were chosen such that no (or only very slight) solvent vapor breakthrough occurred during the adsorption step; thus, $R = 100\%$ and $y_p = 0$ for most runs. Furthermore, since the purpose of this study was to investigate the heat transfer and adsorbate heat capacity effects, the operating conditions, such as the pressure ratio, purge to feed ratio, feed concentration, feed flow rate, and cycle time were fixed (see Table 1). In such a case, E was not expected to change significantly (Liu and Ritter, 1996); therefore, the process performance was judged mainly in terms of the BCF.

Mathematical Model and Model Inputs

Mathematical Model

The rigorous mathematical model of this PSA-SVR process accounted for finite heat and mass transfer resistances, integration of the pressurization and blowdown steps, and gas phase velocity variations during each step. It also accounted for the temperature-dependence of the gas phase physical properties. Different from most PSA models in the literature, and to investigate the adsorbate heat capacity effect, the heat capacity of the adsorbed phase was included in the energy balance. The assumptions used to derive the model included: inert carrier gas and adsorbent; single component feed; negligible column pressure drop; ideal gas behavior; no radial gradients, and no axial dispersion and heat conduction; thermal equilibrium between gas phase and adsorbent; and temperature-independent adsorbent properties. Mass and heat transfer were accounted for, respectively, by the linear driving force (LDF) approximation, and an overall heat transfer coefficient.

The component and total mass balances were given by

$$\frac{\partial y}{\partial t} + u\frac{\partial y}{\partial z} + (1-y)\frac{(1-\varepsilon)}{\varepsilon}\frac{RT}{P}\rho_p\frac{\partial q}{\partial t} = 0 \tag{2}$$

$$\frac{\partial u}{\partial z} - \frac{1}{T}\frac{\partial T}{\partial t} + \frac{1}{P}\frac{\partial P}{\partial t} - \frac{u}{T}\frac{\partial T}{\partial z} + \frac{(1-\varepsilon)}{\varepsilon}\frac{RT}{P}\rho_p\frac{\partial q}{\partial t} = 0 \tag{3}$$

where $\partial q/\partial t$ was based on the LDF approximation as:

$$\frac{\partial q}{\partial t} = k(q^* - q) \tag{4}$$

The energy balance was given by

$$\frac{\partial(uCp_g)}{\partial z} + \left(\frac{Cp_g}{P}\frac{\partial P}{\partial t} + \frac{\partial Cp_g}{\partial t}\right) + \rho_p Cp_s\frac{1-\varepsilon}{\varepsilon}\frac{R}{P}\frac{\partial T}{\partial t} + \frac{1-\varepsilon}{\varepsilon}\frac{R}{P}\rho_p\frac{\partial[q(Cp_aT + \Delta H)]}{\partial t} + \frac{2h}{\varepsilon r_b}\frac{R}{P}(T - T_0) = 0 \tag{5}$$

Table 2. Values of the parameters used in the model equations.

	Parameters for the gas phase heat capacity, Cp_g (kJ/(mol K))			
	$A \times 10^2$	$B \times 10^4$	$C \times 10^7$	$D \times 10^{11}$
n-Butane	0.948	3.310	−1.107	−0.282
Nitrogen	3.112	−0.136	0.268	1.167

	Parameters for the three process Langmuir model for *n*-butane on BAX carbon			
	q_m	A	b_0	B
Process 1	0.004814	1497.18	0.0006985	3184.0
Process 2	0.22621	737.289	0.0002652	2205.951
Process 3	0.17997	1067.552	0.0023777	400.457

	Parameters for the pressure history, P (kPa)			
	p_0	p_1	$p_2 \times 10^4$	$p_3 \times 10^6$
Pressurization	15.123	0.766	1.144	−0.542
Blowdown	113.604	−2.674	287.002	−108.291
Purge	21.845	−0.029	0.291	0.0000139

The gas phase heat capacity was given by

$$Cp_g = yCp_{g1} + (1-y)Cp_{g2} \tag{6}$$

where subscripts 1 and 2 denote pure *n*-butane vapor and pure inert carrier gas (nitrogen). A cubic temperature dependence for the gas phase heat capacities was assumed (Walas, 1985), and given by

$$Cp_{gi} = A_i + B_i T + C_i T^2 + D_i T^3 \quad (i = 1, 2) \tag{7}$$

The heat capacity parameters are given in Table 2. The initial and boundary conditions are listed below; they were applied to every cycle.

Step I: at $t = 0$: $y = y_{\mathrm{IV}}$, $T = T_{\mathrm{IV}}$, $q = q_{\mathrm{IV}}$, for all z
at $z = 0$: $u = 0$ for all t
at $z = L$: $y = 0$, $T = T_0$ for all t

Step II: at $t = 0$: $y = y_{\mathrm{I}}$, $T = T_{\mathrm{I}}$, $q = q_{\mathrm{I}}$, for all z
at $z = 0$: $y = y_f$, $T = T_f$, $u = u_f$ for all t

Step III: at $t = 0$: $y = y_{\mathrm{II}}$, $T = T_{\mathrm{II}}$, $q = q_{\mathrm{II}}$, for all z
at $z = L$: $u = 0$ for all t

Step IV: at $t = 0$: $y = y_{\mathrm{III}}$, $T = T_{\mathrm{III}}$, $q = q_{\mathrm{III}}$, for all z
at $z = L$: $y = 0$, $T = T_0$, $u = u_p$ for all t

Model Inputs

Adsorption isotherms at 293.2 and 323.2 K for the *n*-butane-BAX activated carbon system were provided by the Westvaco Charleston Research Center (Tolles, 1996). They are displayed in Fig. 1. Because these isotherms covered a very broad pressure range, it was very difficult to find an isotherm model that could fit the data. The only model that worked satisfactorily and had a proper Henry's law limit was developed recently by Drago et al. (1996). It is referred to as the three

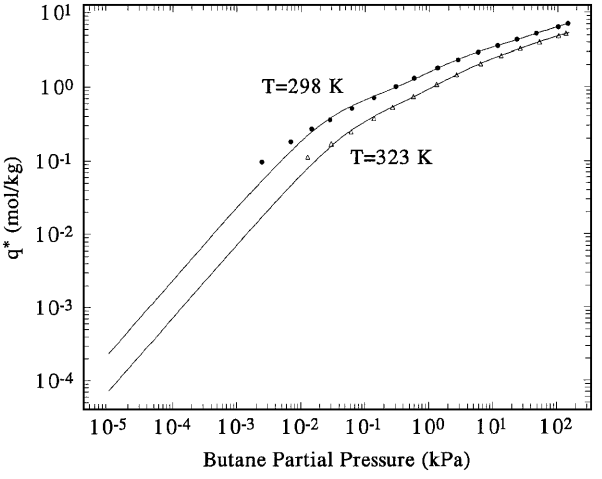

Figure 1. Adsorption equilibrium isotherms of *n*-butane vapor on BAX activated carbon.

process Langmuir model (TPLM). Upon modification of this model to include temperature independent parameters, the following empirical relationships were developed:

$$q^* = \sum_{i=1}^{3} \frac{q_{mi} b_i P y}{1 + b_i P y} \quad i = 1, 2, 3 \tag{8}$$

$$q_{mi} = q_{0i} \exp\left(\frac{A_i}{T}\right) \tag{9}$$

$$b_i = b_{0i} \exp\left(\frac{B_i}{T}\right) \tag{10}$$

This modified TPLM was fitted simultaneously to both of the *n*-butane-BAX activated carbon isotherms to determine the 12 parameters using nonlinear regression. The average relative error (ARE), defined as

$$\text{ARE} = \frac{100}{N} \sum_{i=1}^{N} \text{abs}\left(\frac{q_{\text{exp},i} - q_{\text{cal},i}}{q_{\text{exp},i}}\right)\% \tag{11}$$

was very low at only 5.3%. This excellent fit is shown in Fig. 1, which compares the model correlation (solid lines) with the experimental data (symbols). The modified TPLM parameters are given in Table 2.

The pressure history was also required as input to the PSA model. It was obtained from a preliminary experiment performed under similar process conditions (Liu et al. 1997); this pressure history is shown in Fig. 2 for two periodic-state cycles. In the model, the pressure history was held constant at P_H during the adsorption step; and it was fitted to polynomials of the following form

$$P = p_0 + p_1 t + p_2 t^2 + p_3 t^3 \tag{12}$$

during the other three steps. The polynomial parameters are given in Table 2.

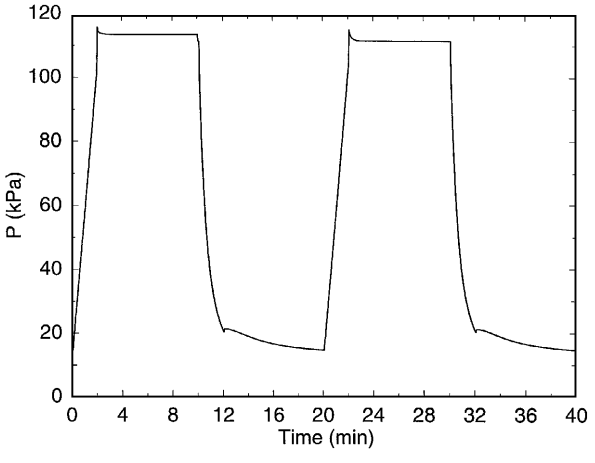

Figure 2. Experimental pressure history from one column during two complete cycles (note that in all simulations the pressure during step II was held constant).

A constant heat of adsorption (ΔH) was used in the energy balance. It was determined by averaging the isosteric heat of adsorption obtained at different loadings from the adsorption isotherms, as outlined by Valenzuela and Myers (1989). The mass transfer coefficient (k) was calculated according to $k = 15 D_e / r_p^2$, where D_e was measured experimentally by the uptake method proposed by Ruthven (1992). The uptake experiments were carried out gravimetrically at different *n*-butane mole fractions ranging from 5 to 100%. An average D_e was used to calculate k using a pellet radius of 1.05 mm.

Equations (2) to (10) and (12), along with the set of initial and boundary conditions, represent the comprehensive mathematical model that was used to study heat effects in a PSA-SVR process. The model was solved using a finite difference scheme starting from step II and a clean bed. Details of the solution method are given elsewhere (Liu and Ritter, 1996).

Results and Discussion

For any non-isothermal PSA operation, it would be advantageous to carry out the adsorption step at the lowest possible temperature to maximize the capacity, and to carry out the desorption step at the highest possible temperature to maximize the extent of regeneration. But for PSA, this is difficult to accomplish because there are no external sources of heating or cooling; and the heating and cooling that comes from the heat of adsorption generally opposes this kind of operation because the beds actually heat up during adsorption and cool down during desorption. These characteristic heat effects in PSA systems have led to some general beliefs that are worth discussing before analyzing the results obtained from this study.

The first belief is that isothermal operation should always lead to the best process performance; thus, conversely, adiabatic operation should always lead to the worst (Chihara and Suzuki, 1983; Yang, 1987). The second belief is that it is always advantageous to retain the heat of adsorption within the bed during the adsorption step so that it may be used to assist

Table 3. Values of the heat transfer coefficient (h) [kJ/(m^2 s K)] and adsorbate heat capacity (Cp_a) [kJ/(mol K)] used in each run; and the results of each run in terms of the process performance indicators, BCF and E.

	h_1: 0.0000		h_2: 0.00067		h_3: 0.0025		h_4: 0.00989		h_5: 0.0523		h_6: 0.2000		h_7: 0.5000		h_8: 10.0000	
	BCF	E	BCF	E	BCF	E	BCF	E	BCF	E	BCF	E	BCF	E	BCF	E
Cp_{a1}: 0.0000	0.634	2.689[a]	0.635	2.667[b]	0.684	2.670[c]	0.771	2.736[d]	0.732	2.768	0.487	2.749	0.367	2.729	0.292	2.677
Cp_{a2}: 0.0668	0.474	2.691	0.480	2.663	0.511	2.664	0.591	2.695[e]	0.665	2.757	0.426	2.737	0.344	2.716	0.292	2.677
Cp_{a3}: 0.0986	0.416	2.692	0.426	2.664	0.451	2.664	0.509	2.688	0.576	2.746	0.398	2.734	0.333	2.710	0.292	2.677
Cp_{a4}: 0.1161	0.388	2.692	0.401	2.665	0.422	2.665	0.470	2.685	0.531	2.740	0.383	2.729	0.327	2.706	0.292	2.677
Cp_{a5}: 0.1335	0.363	2.691	0.378	2.666	0.396	2.665	0.428	2.681	0.488	2.733	0.327	2.716	0.322	2.702	0.292	2.677

[a] $y_p = 0.19$ ppb for this run. [b] $y_p = 0.2$ ppb for this run. [c] $y_p = 0.011$ ppm for this run. [d] $y_p = 0.877$ ppm for this run. [e] $y_p = 0.0625$ ppm for this run. For all other runs, $y_p = 0.0$.

regeneration during the desorption step (Leavitt, 1962; White and Barkley, 1984). Clearly, these two statements are somewhat contradictory. In fact, the results obtained in this study show very clearly that these general comments about non-isothermal operation may not be correct for all PSA processes.

To prove or disprove these general claims, forty simulations were performed to investigate the interrelated effects of the overall heat transfer coefficient (h) and the adsorbate heat capacity (Cp_a) on the PSA-SVR process dynamics and performance. The values of h and Cp_a utilized in each run are given in Table 3, along with the resulting process performance indicators, i.e., the BCF and E. For each Cp_a, eight different heat transfer coefficients were selected, which ranged from $h = 0$ (adiabatic condition) to $h = 10$ kJ/(m^2 s K) (isothermal condition). Due to the complex behavior of Cp_a and the uncertainty in its actual value (Barrer, 1978), five different values of Cp_a were used to investigate how Cp_a affects the simulation results. They ranged from zero to the heat capacity of *n*-butane vapor [0.0986 kJ/(mol K)] at room temperature to the heat capacity of saturated *n*-butane liquid [0.1335 kJ/(mol K)] at room temperature, with the two other values in between zero and that of the solvent vapor and in between that of the solvent vapor and its saturated liquid.

Effect of the Heat Transfer Coefficient on the Bed Capacity Factor

Figure 3 shows the effect of the heat transfer coefficient, h, on the bed capacity factor, BCF, at different values of the adsorbate heat capacity, Cp_a. Remember, at fixed operating conditions, a larger BCF means that a larger portion of the bed has been contaminated, which necessarily implies a poorer process performance. The effect

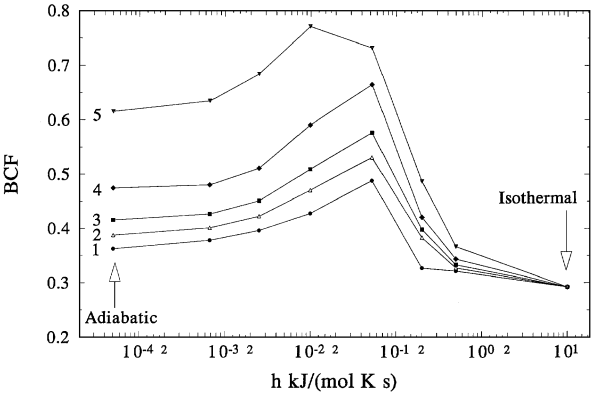

Figure 3. Effects of the heat transfer coefficient (h) and the adsorbed phase heat capacity (Cp_a) on the bed capacity factor (BCF).

of h on the BCF was more complicated than expected. At each Cp_a, when the process was changed from adiabatic to isothermal, the BCFs went through a maximum at an intermediate h. Isothermal operation resulted in the smallest BCF, but adiabatic operation did not result in the largest. In other words, with all other conditions fixed, isothermal operation gave rise to the best performance, but adiabatic operation was surprisingly not the worst. According to the BCFs, the worst PSA-SVR process performance occurred at an intermediate h (the one corresponding to the largest BCF). Figures 4 and 5, which show the temperature and gas phase concentration profiles at the end of the adsorption and purge steps for runs with $Cp_a = 0.1161$ kJ/(mol K) but for five different heat transfer coefficients, were used to explain this unexpected heat effect.

Figure 4 shows that at the end of the adsorption step, the smaller h produced higher temperatures in most of the bed, while at the end of purge step, the smaller h produced lower temperatures, except for the adiabatic

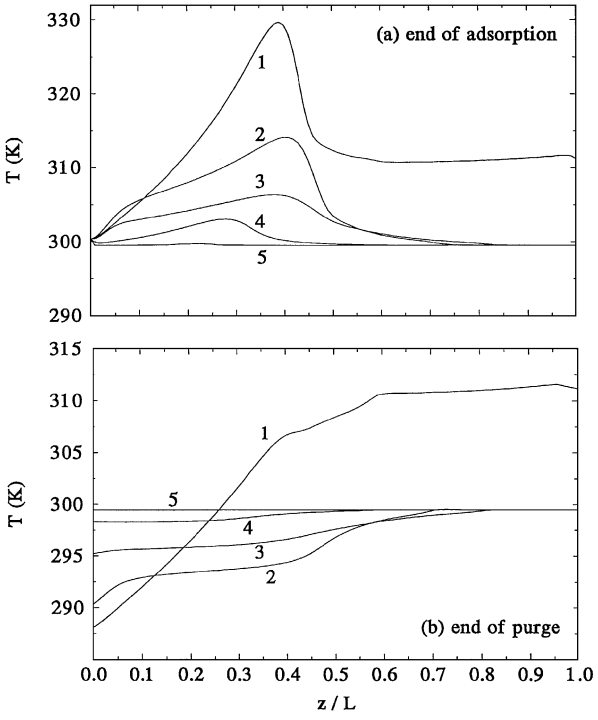

Figure 4. Periodic state temperature profiles at the (a) end of the adsorption step and (b) end of the purge step showing the effects of the heat transfer coefficient (h) with the adsorbed phase heat capacity (Cp_a) held constant. Curves 1, 2, 3, 4 and 5 (i.e., h increasing at constant Cp_a) correspond to profiles of runs h_1-Cp_{a4}, h_4-Cp_{a4}, h_5-Cp_{a4}, h_6-Cp_{a4} and h_8-Cp_{a4} in Table 3, respectively.

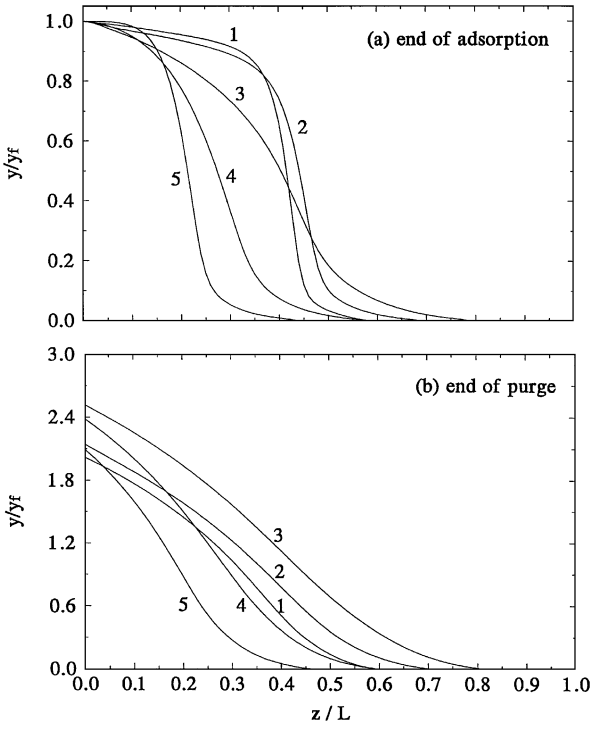

Figure 5. Periodic state concentration profiles at the (a) end of the adsorption step and (b) end of the purge step showing the effects of the heat transfer coefficient (h) with the adsorbed phase heat capacity (Cp_a) held constant. Curves 1, 2, 3, 4 and 5 (i.e., h increasing at constant Cp_a) correspond to profiles of runs h_1-Cp_{a4}, h_4-Cp_{a4}, h_5-Cp_{a4}, h_6-Cp_{a4} and h_8-Cp_{a4} in Table 3, respectively.

case. Under the adiabatic condition, the heat released during the adsorption step had nowhere to escape and could only be convected to the light product end of the bed. During the purge step, this large amount of heat, coupled with the high temperature purge gas coming from the light product of the adsorption step of the other bed, kept most of the bed at higher temperatures. However, these seemingly consistent trends could not explain the gas phase concentration profiles shown in Fig. 5.

For example, even though the temperatures in Fig. 4(a) increased consistently with decreasing h, the corresponding gas phase concentration profiles exhibited far more complex behavior with distinct spreading followed by sharpening of the wave front with decreasing h. Moreover, the most dispersed profile (curve 3) corresponded to the apparent maximum in Fig. 3; and thus, the largest BCF of the five runs (see Table 3). These dispersed profiles could be related to the degree of isotherm nonlinearity, as manifested through the effect of temperature on the adsorption isotherm. However, investigation of the isotherm-nonlinearity is beyond the scope of this work, because the objective here was to study heat effects in an actual PSA-SVR process; namely, the *n*-butane vapor-BAX activated carbon system. Figure 4(a) also shows that some of the heat of adsorption was retained within the bed, as evidenced by the elevated temperatures. But higher temperatures, in general, correspond to lower loadings, which necessarily push the wave front further down the bed. However, depending on the heat transfer characteristics, if enough heat is retained within the bed during the adsorption step, it could assist in regenerating the column during the desorption step, but only if cooling during the desorption step does not counteract this adsorption energy. Clearly, these coupled and opposing effects, including effects from the degree of isotherm nonlinearity, gave rise to the complex behavior shown in Fig. 3.

For the adiabatic case, the retained heat of adsorption was enough to overcome the desorption cooling (Fig. 4(b)); thus, significant desorption took place,

which caused the gas phase concentration profile at the end of the purge step (curve 1, Fig. 5(b)) to lie somewhere in between those of the isothermal (curve 5) and non-isothermal cases (curve 3). At some intermediate h, e.g., in this case at $h = 0.0523$ kJ/(m^2 s K), the heat of adsorption was not enough to overcome the desorption cooling. This gave rise to the largest BCF and thus the worst process performance. These trends are exemplified by the variations of the bed temperatures, and gas and adsorbed phase loadings shown in Fig. 6 for a complete cycle at an axial position within the wave front region where significant adsorption and desorption took place.

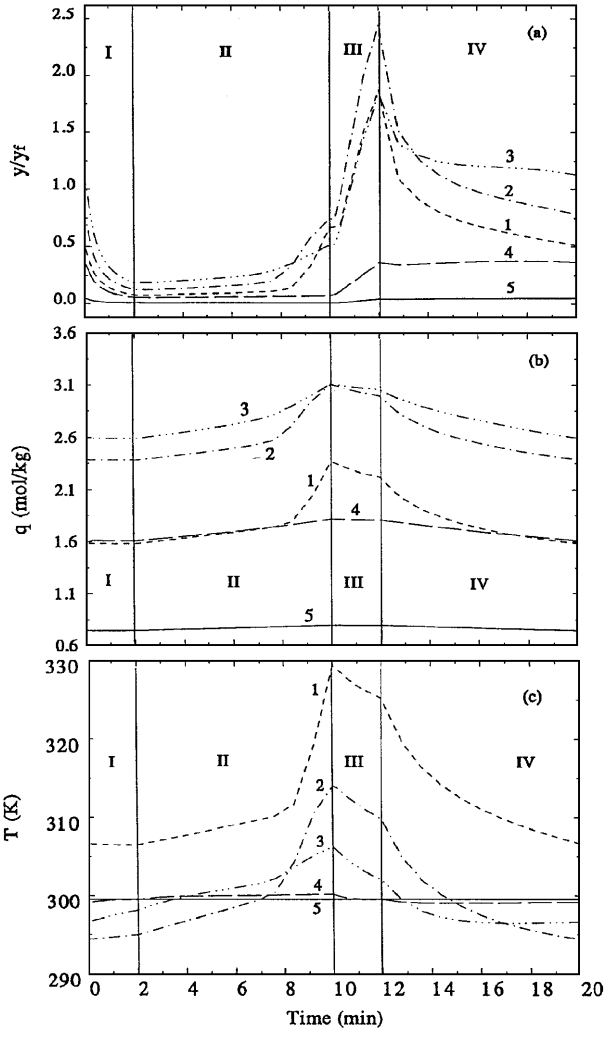

Figure 6. Dependent variable variations during a periodic state cycle at $z/L = 0.40$ showing the effects of the heat transfer coefficient (h) with the adsorbed phase heat capacity (Cp_a) held constant: (a) gas phase concentration, (b) adsorbed phase loading and (c) temperature. Curves 1, 2, 3, 4 and 5 (i.e., h increasing at constant Cp_a) correspond to runs h_1-Cp_{a4}, h_4-Cp_{a4}, h_5-Cp_{a4}, h_6-Cp_{a4} and h_8-Cp_{a4} in Table 3, respectively.

At $z/L = 0.4$, the run with a smaller h, e.g., curve 2, exhibited lower temperatures during most of the adsorption step and higher temperatures during most of the purge step, compared to the run with a larger h, e.g., curve 3, which corresponded to the maximum BCF. It was this temperature variation during the cycle that enhanced the adsorption and desorption for the process with a smaller h, thereby giving rise to a smaller BCF. However, when h was greater than the "critical" h (the one corresponding to the maximum BCF), e.g., curve 4, the temperatures were lower during most of the adsorption step and higher during most of the purge step, because of the small heat transfer resistance compared to the run with the "critical" h. Therefore, this h also resulted in a smaller BCF.

So, for a range of h and starting at the isothermal condition, as the process became more nonisothermal, adsorption heating and desorption cooling were detrimental to the process performance; and therefore any heat retained in the bed was not very useful. Clearly, it would be advantageous to find process conditions that would dissipate the heat, thereby causing the process to operate more isothermally. However, after some critical value of h was reached, e.g., at $h = 0.0523$ kJ/(m^2 s K), adsorption heating and heat retention dominated the process dynamics and overwhelmed the detrimental effects of desorption cooling. Under these circumstances, it would be advantageous and easier to find process conditions that would cause the process to operate more adiabatically than isothermally.

Effect of the Adsorbate Heat Capacity on the Bed Capacity Factor

Figure 3 shows that for all of the non-isothermal cases, a larger Cp_a improved the process performance, according to the BCF. This effect was easy to understand, because the adsorbed phase works as a heat sink during the adsorption step. It stores some of the heat released during the adsorption step, which effectively decreases the net temperature rise in the bed. During the desorption step, it releases some of the stored heat, which effectively decreases the net temperature fall in the bed. So, in effect, the larger the Cp_a, the smaller the temperature swings, and the closer the PSA system to isothermal operation. This argument is clearly illustrated in Figs. 7 and 8, which display the temperature and gas phase concentration profiles at the end of the adsorption and purge steps for runs with

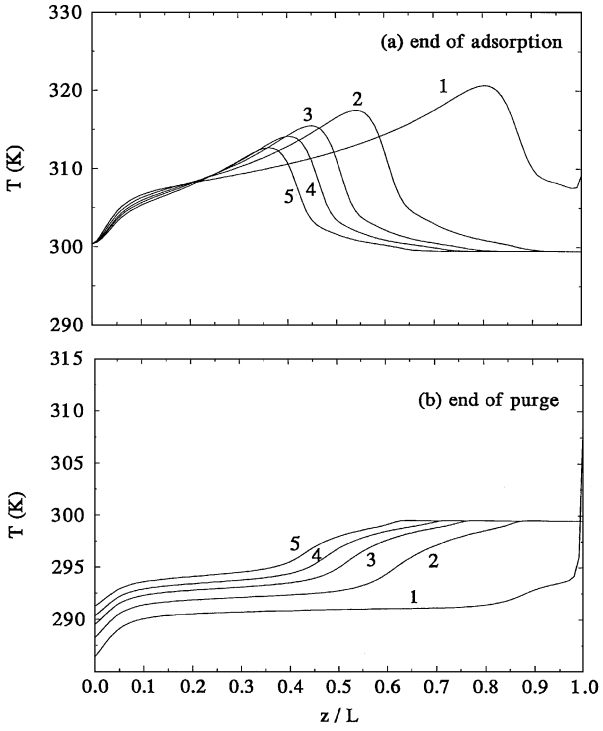

Figure 7. Periodic state temperature profiles at the (a) end of the adsorption step and (b) end of the purge step showing the effects of the adsorbed phase heat capacity (Cp_a) with the heat transfer coefficient (h) held constant. Curves 1, 2, 3, 4 and 5 (i.e., Cp_a increasing at constant h) correspond to profiles of runs h_4-Cp_{a1}, h_4-Cp_{a2}, h_4-Cp_{a3}, h_4-Cp_{a4} and h_4-Cp_{a5} in Table 3, respectively.

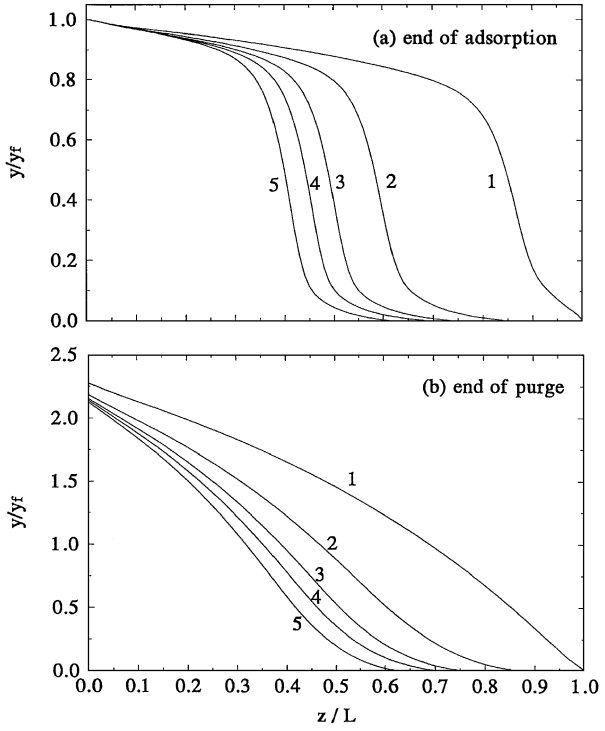

Figure 8. Periodic state concentration profiles at the (a) end of the adsorption step and (b) end of the purge step showing the effects of the adsorbed phase heat capacity (Cp_a) with the heat transfer coefficient (h) held constant. Curves 1, 2, 3, 4 and 5 (i.e., Cp_a increasing at constant h) correspond to profiles of runs h_4-Cp_{a1}, h_4-Cp_{a2}, h_4-Cp_{a3}, h_4-Cp_{a4} and h_4-Cp_{a5} in Table 3, respectively.

$h = 0.00989$ kJ/(mol K) but for all five different adsorbate heat capacities.

As Cp_a decreased, the temperature swings increased over much of the bed, which decreased the bed capacity during the adsorption step and increased it during the desorption step, thereby increasing the depth of penetration of the concentration wave front. This trend is very apparent in Fig. 9, which displays the variations of the bed temperature, and gas and adsorbed phase loadings during a complete periodic state cycle, at an axial position where the bed was nearly saturated for all values of the Cp_a, i.e., at $z/L = 0.05$. For increasing Cp_a, the temperatures were lower during the adsorption step and higher during the desorption step, which manifested as an increased capacity during the adsorption step and a decreased capacity during the desorption step. This behavior was not unique to the periodic state, however. It also propagated through the transient periods starting from a completely clean bed. During each cycle, on the approach to the periodic state, the adsorption temperature was higher and the desorption temperature was lower for decreasing Cp_a, thereby giving rise to less capacity during adsorption (increased depth of penetration) and more capacity during desorption (less regeneration). These trends continued cycle by cycle, resulting in a larger periodic state BCF with decreasing Cp_a, as shown in Fig. 3.

The results in Table 3 also show that, for the five runs shown in Fig. 7, i.e., when $h = 0.0523$ kJ/(m^2 s K), the BCF increased by 18% with $Cp_a = Cp_g$ compared to $Cp_a = Cp_l$. The change in the BCF was even more striking with $Cp_a = 0.0$, i.e., the BCF increased by 80% compared to $Cp_a = Cp_l$. Moreover, Fig. 3 shows that the effects of Cp_a on the BCF depended on the heat transfer characteristics of the PSA system. When h increased, so that the process approached the isothermal condition, the effects of Cp_a faded, because heat was more easily transferred to and from the system. Therefore, the temperature swings necessarily decreased, as shown in Figs. 4 and 7. These results indicate very clearly that the effects of h and Cp_a are uniquely coupled; thus knowing their magnitudes is paramount to obtaining accurate predictions from a PSA-SVR model.

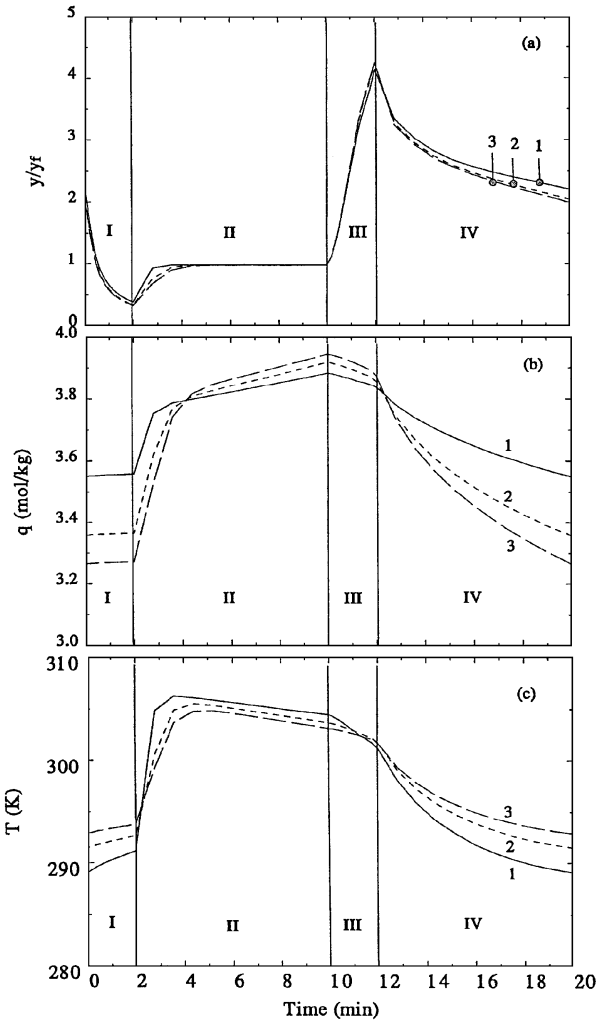

Figure 9. Dependent variable variations during a periodic state cycle at $z/L = 0.05$ showing the effects of the adsorbed phase heat capacity (Cp_a) with the heat transfer coefficient (h) held constant: (a) gas phase concentration, (b) adsorbed phase loading and (c) temperature. Curves 1, 2 and 3 (i.e., Cp_a increasing at constant h) correspond to runs h_4-Cp_{a1}, h_4-Cp_{a3} and h_4-Cp_{a5} in Table 3, respectively.

Heat Effects on the Solvent Vapor Enrichment

Table 3 shows that the E predicted by all of the runs did not change very much. The largest percent difference of the Es from all of these runs was approximately 3.5%. This was expected for this essentially breakthrough-free PSA process. For such PSA processes, the necessary condition for the periodic state to exist is that the amount of solvent vapor recovered during the blowdown and purge steps must equal the amount of solvent vapor fed into the bed during each cycle. Therefore, E depends mainly on the pressure and purge to feed ratios (Subramanian and Ritter, 1997), which were held constant in all cases. Thus, the subtle changes in E with h were most likely due to the subtle changes in the gas phase velocity and temperature at the exit of the bed during the blowdown and purge steps.

According to the ideal gas law, any changes in temperature or velocity would certainly affect the solvent vapor mole fraction and thus E. However, if the process conditions are changed so that breakthrough occurs during the adsorption step, h would most definitely affect E because of its effect on the BCF. In such cases, a heat transfer coefficient that results in a larger BCF would decrease E because a larger portion of the concentration wave front would break through the bed (Liu and Ritter, 1996).

Heat Effects at Different Cycle Times and Feed Concentrations

There are many parameters, including the process and operating conditions, that affect the PSA-SVR process performance. Most of these effects have been studied by Liu and Ritter (1996, 1997a). However, whether or not the heat effect becomes more pronounced with changes in the cycle time and the feed concentration remains unknown. The best way to obtain this information is to perform a factorial analysis, among which the two-level factorial design is the simplest. For specific details on the factorial design method, refer to Box et al. (1978), Lochner and Matar (1990) and Liu and Ritter (1997a).

The goal here was to perform a two-level factorial analysis to determine the effects of Cp_a at different cycle times (t_c) and feed concentrations (y_f). Two levels of each of the three parameters (Cp_a, t_c and y_f) were selected. Eight runs were needed for this two-level, three-factor, full factorial analysis. The design matrix and the results for each run, in terms of the BCF and E, and the effects of each factor and factor interactions, are given in Table 4 along with the selected factor levels. All of these runs were carried out using $h = 0.00067$ kJ/(m^2 s K). Also, for $t_c = 5$ min compared to $t_c = 20$ min, the cycle step times were scaled down proportionally to ensure the same throughput.

Note that the heat transfer coefficient could not be included in this simple two-level analysis because of its non-monotonous behavior (see Fig. 3). Nevertheless, Liu and Ritter (1997a) showed that h does not interact

Table 4. Two-level three-factor factorial design matrix and process performance indicators*.

	Factor and interaction levels							Responses	
Run no.	t_c	y_f	Cp_a	t_c-y_f	t_c-Cp_a	y_f-Cp_a	t_c-y_f-Cp_a	BCF	E
a	−	−	−	+	+	+	−	0.176	2.437
b	−	−	+	+	−	−	+	0.137	2.459
c	−	+	−	−	+	−	+	0.186	1.899
d	−	+	+	−	−	+	−	0.138	1.915
e	+	−	−	−	−	+	+	0.635	2.666
f	+	−	+	−	+	−	−	0.378	2.666
g	+	+	−	+	−	−	−	0.712	2.066
h	+	+	+	+	+	+	+	0.404	2.049
(−) Aver. E	2.177	2.557	2.267	2.287	2.277	2.273	2.271		
(+) Aver. E	2.362	1.982	2.272	2.253	2.263	2.267	2.268		
Effect on E	0.185	−0.575	0.005	−0.034	−0.014	−0.006	−0.003		
(−) Aver. BCF	0.159	0.331	0.427	0.334	0.406	0.353	0.351		
(+) Aver. BCF	0.532	0.360	0.264	0.357	0.286	0.338	0.341		
Effect on BCF	0.373	0.029	−0.163	0.023	−0.120	−0.015	−0.010		

*Factors and levels: t_c (min): (+) 20, (−) 5; y_f (%) : (+) 30, (−) 20; Cp_a (kJ/mol K): (+) 0.13351, (−) 0.0000, where (−) represents the low level and (+) represents the high level.

with the other parameters, such as the feed concentration, pressure ratio, purge to feed ratio, pressure level, feed flow rate, cycle time and bed dimension, i.e., the effect of h on the process performance does not depend on the levels of these other parameters. So, it would not be expected to interact with t_c or y_f here. It should also be pointed out that the PSA-SVR process performance goes through a maximum as t_c increases (Liu and Ritter, 1996). However, this maximum seemingly occurs at the onset of breakthrough into the light product. In this factorial study, the process conditions were chosen such that no breakthrough occurred, thereby avoiding the non-monotonous behavior.

The effects of Cp_a, t_c and y_f on the BCF are displayed in Fig. 10, in terms of a normal plot. Four points, other than those representing the main effects of t_c and Cp_a, and the interaction effect of t_c-Cp_a, formed a straight line. According to the normal plot method (Lochner and Matar, 1990; Liu and Ritter, 1997a), this indicated that only these three effects were significant. Moreover, since the effect of the t_c-Cp_a interaction was significant, i.e., the effect of Cp_a on the BCF depended on the levels of t_c and vice versa, the main effects (i.e., the effects of the individual factors) of Cp_a and t_c could not be interpreted separately. Rather, their effects had to be interpreted according to their interaction effect (Lochner and Matar, 1990). To facilitate

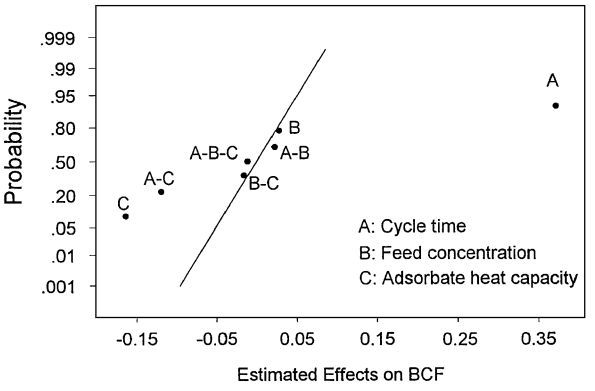

Figure 10. Normal probability plot for the estimated effects on the bed capacity factor (BCF).

this interpretation, a Cp_a-t_c factor interaction graph was constructed; it is shown in Fig. 11.

The two lines are clearly not parallel, which indicated that the effect of each factor depended on the level of the other factor. For example, for the shorter cycle time ($t_c = 5$ min), the models with $Cp_a = 0$ predicted an average BCF of 0.181, while the models with $Cp_a = Cp_l$ predicted 0.1375, a 24.0% decrease. For the longer cycle time ($t_c = 20$ min), the models with $Cp_a = 0$ predicted an average BCF of 0.674, while the models with $Cp_a = Cp_l$ predicted 0.391, a 42.0%

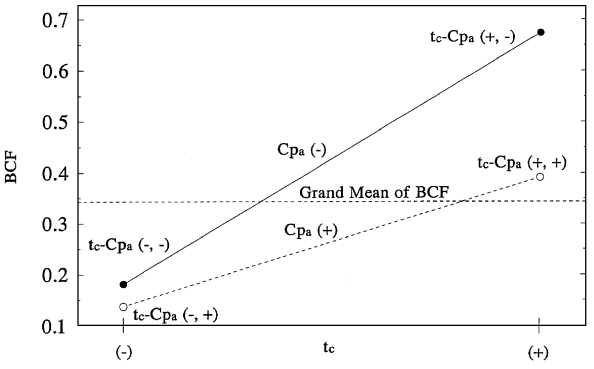

Figure 11. Interaction plot for the effects of the adsorbate heat capacity (Cp_a) and cycle time (t_c) on the bed capacity factor (BCF).

decrease. This meant that including Cp_a in the model had a much larger effect on the BCF as t_c increased. Similarly, for $Cp_a = 0$, the longer t_c produced an average BCF of 0.674, 272.4% higher compared to the shorter t_c (BCF = 0.181). However, for $Cp_a = Cp_l$, the increase in the BCF was only 184.4% (from 0.1375 to 0.391) when changing t_c from 5 to 20 min. This result suggested that when Cp_a was included in the model, the effect of the cycle time on the BCF was reduced.

Also, according to Fig. 11, a longer t_c always produced a larger BCF because of the larger amount of feed that was fed into the bed during a cycle; and a larger Cp_a always resulted in a smaller BCF, which was consistent with the previous discussion. Finally, increasing y_f from 20 to 30% also increased the BCF, but the increase was small compared to the effects of Cp_a and t_c.

The effects of Cp_a, t_c and y_f on E are displayed in Fig. 12, also in terms of a normal plot. Only t_c and

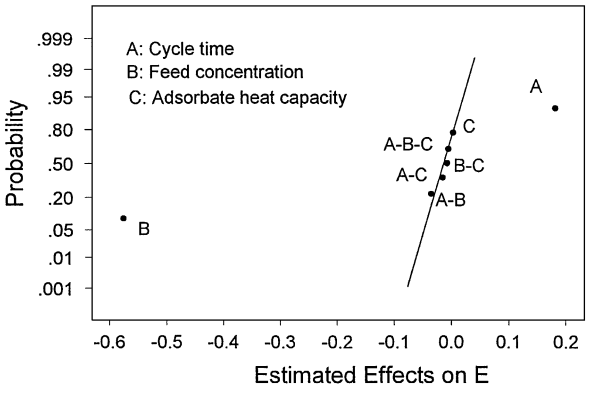

Figure 12. Normal probability plot for the estimated effects on the solvent vapor enrichment (E).

y_f affected E; the effects of Cp_a and all interaction effects were insignificant. Table 4 shows that increasing t_c from 5 to 20 min increased E from an average of 2.177 to an average of 2.362, whereas increasing y_f from 20 to 30% decreased E from an average of 2.557 to an average of 1.982. The minimal effect of Cp_a on E was again caused mainly by the no breakthrough constraint used in all of these simulations.

Conclusions

Periodic state heat effects in a PSA-SVR process were investigated by computer simulation. The emphasis was placed on the convoluted effects of the heat transfer coefficient (h) and the adsorbed phase heat capacity (Cp_a) on the bed capacity factor (BCF), where the effects of Cp_a have been largely overlooked by most researchers investigating PSA processes using mathematical models. Overall, the results showed that, depending on the heat transfer characteristics of the PSA system, retention of the heat of adsorption in the bed may be advantageous or it may be detrimental to the process performance, and adiabatic operation may not lead to the worst process performance.

Specific results showed that the effects of the heat transfer characteristics on the process dynamics and performance were very complicated. In terms of the BCF, isothermal operation always gave the best performance, whereas adiabatic operation was not the worst. The poorest performance, corresponding to the largest BCF, was given by a process using an intermediate h. This striking result was also independent of the value used for Cp_a. Moreover, the larger the Cp_a the better the process performance, but the magnitude of the improvement depended on the value of h. A 2^3 full factorial analysis also showed that the effect of Cp_a on the BCF depended on the cycle time. Including Cp_a or not in the model resulted in much larger differences in the BCFs as the cycle time increased. These trends show very clearly that accurate predictions from a PSA-SVR model rely heavily on knowing the values of h and Cp_a. Many correlations exist to estimate the value of h; however, obtaining an accurate value of Cp_a is not trivial, based on the current state of knowledge of the Cp_a.

Nomenclature

A Parameter in gas phase heat capacity — correlation

B	Parameter in gas phase heat capacity correlation	—
b, b_0	Isotherm parameters	$m^3/(mol\ K^{0.5})$
C	Parameter in gas phase heat capacity correlation	—
Cp	Heat capacity	kJ/(kg K)
D	Parameter in gas phase heat capacity correlation	—
E	Enrichment	
ΔH	Heat of adsorption	kJ/mole
h	Overall heat transfer coefficient	$kJ/(m^2\ s\ K)$
k	Mass transfer coefficient	s^{-1}
L	Bed length	m
N	Total number of experimental data points	—
P	Pressure	kPa
q	Amount adsorbed	mol/kg
q_m, q_0	Parameters in adsorption equilibrium isotherm	mol/kg
q^*	Equilibrium amount adsorbed	mol/kg
r_b	Bed radius	m
R	Gas constant or recovery	—
T	Temperature	K
T_0	Ambient temperature	K
t	Time	s
u	Interstitial velocity	m/s
V	Volumetric flow rate	m^3/s
y	Gas phase mole fraction	—
z	Axial position	m

Greek Symbols

α	Pressure ratio	—
ρ	Density	kg/m^3
ε	Bed void fraction	—
γ	Purge to feed ratio	—

Subscripts

1	Solvent vapor component
2	Inert carrier gas component
a	Adsorption, or adsorbate
b	Bed
c	Cycle
cal	Calculated
exp	Experimental
f	Feed
g	Gas phase
H	High
i	Index
L	Low
l	Liquid phase
p	Light product, or purge, or pellet
s	Solid phase or step
I, II, III, IV	Step numbers

Acknowledgment

The authors gratefully acknowledge financial support from the National Science Foundation under Grants CTS-9410630 and OSR-9108 772-004, and from the Westvaco Charleston Research Center.

References

Barrer, R.M., *Zeolites and Clay Minerals as Sorbents and Melecular Sieves*, Chap. 5, Academic Press, London, 1978.

Berezin, G.I. and A.V. Kiselev, "Dependence of Heat Capacity of Adsorbate on Surface Coverage on the BET Theory Assumptions," *J. Colloid Interface Sci*., **22**, 161–164 (1966).

Box, G.E.P., W.G. Hunter, and J.S. Hunter, *Statistics for Experiments*, John Wiley & Sons, New York, 1978.

Cen, P. and R.T. Yang, "Bulk Gas Separation by Pressure Swing Adsorption," *Ind. Eng. Chem. Fundam*., **25**, 758–767 (1986).

Chihara, K. and Suzuki, M., "Simulation of Nonisothermal Pressure Swing Adsorption," *J. Chem. Eng. Jpn.*, **16**, 53 (1983).

Doong, S.J. and R.T. Yang, "Bulk Separation of Multicomponent Gas Mixture by Pressure Swing Adsorption: Pore/Surface Diffusion and Equilibrium Models," *AIChE J*., **32**, 397–410 (1986).

Drago, R.S., D.S. Burns, and T.J. Lafrenz, "A New Adsorption Model for Analyzing Gas-Solid Equilibria in Porous Materials," *J. Phys. Chem*., **100**(5), 1718–1724 (1996).

Farooq, S., M.M. Hassan, and D.M. Ruthven, "Heat Effects in Pressure Swing Adsorption Systems," *Chem. Eng. Sci*., **43**, 1017–1031 (1988).

Hill, T.L., "Statistical Mechanics of Adsorption. V. Thermodynamics and Heat of Adsorption," *J. Chem. Phys*., **17**, 520–535 (1949).

Kapoor, A. and R.T. Yang, "Separation of Hydrogen-Lean Mixtures for a High-Purity Hydrogen by Vacuum Swing Adsorption," *Sep. Sci. Technol*., **23**, 153–178 (1988).

Kikkinides, E.S., J.A. Ritter, and R.T. Yang, "Pressure Swing Adsorption for Simultaneous Purification and Sorbate Recovery," *J. Chin. Inst. Chem. Eng*., **22**, 399–407 (1991).

Leavitt, F.W., "Non-isothermal Adsorption in Large Fixed Beds," *Chem. Eng. Prog*., **58**(8), 54–59 (1962).

LeVan, M.D., "Pressure Swing Adsorption: Equilibrium Theory for Purification and Enrichment," *Ind. Eng. Chem. Res*., **34**(8), 2655–2660 (1995).

Liu, Y. and J.A. Ritter, "Pressure Swing Adsorption-Solvent Vapor Recovery: Process Dynamics and Parametric Study," *Ind. Eng. Chem. Res*., **35**(7), 2299–2312 (1996).

Liu, Y. and J.A. Ritter, "Fractional Factorial Study of a Pressure Swing Adsorption-Solvent Vapor Recovery Process," *Adsorption*, **3**, 151–163 (1997a).

Liu, Y. and J.A. Ritter, "Evaluation of Model Approximations in Simulating Pressure Swing Adsorption-Solvent Vapor Recovery," *Ind. Eng. Chem. Res.*, **36**(5), 1767–1778 (1997b).

Liu Y., C.E. Holland, and J.A. Ritter, "Solvent Vapor Recovery by Pressure Swing Adsorption-II: Experimental Periodic Performance of the Butane-Activated Carbon System," submitted to *Sep. Sci. Tech.* (1997).

Lochner, R.H. and J.E. Matar, *Designing for Quality: An Introduction to the Best of Taguchi and Western Methods of Statistical Experimental Design*, Quality Resources, New York, ASQC Quality Press, Wisconsin, 1990.

Mahle, J.J., D.K. Friday, and M.D. LeVan, "Pressure Swing Adsorption for Air Purification. 1. Temperature Cycling and Role of Weakly Adsorbed Carrier Gas," *Ind. Eng. Chem. Res.*, **35**(7), 2342–2354 (1996).

Ritter, J.A. and R.T. Yang, "Pressure Swing Adsorption: Experimental and Theoretical Study on Air Purification and Vapor Recovery," *Ind. Eng. Chem. Res.*, **30**, 1023–1032 (1991a).

Ritter, J.A. and R.T. Yang, "Air Purification and Vapor Recovery by Pressure Swing Adsorption: A Comparison of Silicalite and Activated Carbon," *Chem. Eng. Comm.*, **108**, 289–305 (1991b).

Ruthven, D.M., *Principles of Adsorption and Adsorption Processes*, John Wiley & Son, New York, 1984.

Ruthven, D.M., "Diffusion of Oxygen and Nitrogen in Carbon Molecular Sieves," *Chem. Eng. Sci.*, **47**(17/18), 4305–4308 (1992).

Ruthven, D.M., S. Farooq, and K.S. Knaebel, *Pressure Swing Adsorption*, VCH Publishers, New York, 1994.

Sircar, S., "Excess Properties and Thermodynamics of Multicomponent Gas Adsorption," *J. Chem. Soc. Faraday Trans. I*, **81**, 1527–1540 (1985).

Skarstrom, C.W., "Use of Adsorption Phenomena in Automatic Plant-type Gas Analyzers," *Ann. N.Y. Acad. Sci.*, **72**, 751 (1959).

Subramanian, D. and J.A. Ritter, "Equilibrium Theory for Solvent Vapor Recovery by Pressure Swing Adsorption: Analytical Solution for Process Performance," *Chem. Eng. Sci.*, **52**, 3147–3160 (1997).

Tolles, E.D., Westvaco Charleston Research Center, Charleston, SC, personal communication, 1996.

Tondeur, D. and P.C. Wankat, "Gas Purification by Pressure Swing Adsorption," *Sep. Purif. Meth.*, **14**(2), 157 (1985).

Valenzuela, D.P. and A.L. Myers, *Adsorption Equilibrium Data Handbook*, pp. 12–16, Prentice Hall, New Jersey, 1989.

Wankat, P.C., *Large-Scale Adsorption and Chromatography*, Vol. I, CRC Press, Boca Raton, Florida, 1986.

Wankat, P.C. and L.R. Partin, "Process for Recovery of Solvent Vapors with Activated Carbon," *Ind. Eng. Chem. Process Des. Dev.*, **19**, 446–451 (1980).

Walas, S.M., *Phase Equilibria in Chemical Engineering*, Butterworth-Heinemann, Boston, 1985.

White, D.H. and P.G. Barkley, "The Design of Pressure Swing Adsorption Systems," *Chem. Eng. Prog.*, **1**, 25 (1984).

Yang, R.T., *Gas Separation by Adsorption Processes*, Butterworth, London, 1987.

Yang, R.T. and S.J. Doong, "Gas Separation by Pressure Swing Adsorption: A Pore-Diffusion Model for Bulk Separation," *AIChE J.*, **31**, 1829–1842 (1985).